International Journal of Solids and Structures 51 (2014) 3604–3618

Contents lists available at ScienceDirect

International Journal of Solids and Structures

journal homepage: www.elsevier.com/locate/ijsolstr

Shock wave propagation through a model one dimensional heterogeneous medium

Vinamra Agrawal, Kaushik Bhattacharya *

Division of Engineering and Applied Science, California Institute of Technology, Pasadena, CA 91125, USA

ARTICLE INFO

Article history:
Received 26 December 2013
Received in revised form 15 May 2014
Available online 15 July 2014

Keywords:
Heterogeneous materials
Shock waves
Impact
Hugoniot

ABSTRACT

We study the problem of impact-induced shock wave propagation through a model one-dimensional heterogeneous medium. This medium is made of a model material with spatially varying parameters such that it is heterogeneous to shock waves but homogeneous to elastic waves. Using the jump conditions and maximal dissipation criteria, we obtain the exact solution to the shock propagation problem. We use it to study how the nature of the heterogeneity changes material response, the structure of the shock front and the dissipation.

1. Introduction

Shock wave propagation in solids has been extensively studied for a number of decades, see for example Davison (2008) and the references there. Shocks are described as a moving front across which the stress, strain and particle velocity suffer a discontinuity. They occur when subjected to large deformations at high deformation rates as a result of the nonlinear nature of the equation of state.

While shocks are idealized as a discontinuity, in reality they have a structure where the state of stress varies sharply but smoothly across a narrow region to connect to the limiting states. This structure is commonly attributed to time-dependent inelastic process like viscoelasticity (Band, 1960), viscoplasticity (Swegle and Grady, 1985; Armstrong et al., 2007; Johnson and Barker, 1969), twinning etc. In particular, Swegle and Grady (1985) compiled experimental observations of a wide range of metals and showed that the shock structure follows an universal fourth power law – the peak strain rate in the shock is proportional to the fourth power of the jump in stress across the shock wave. They also proposed a viscoplastic constitutive law consistent with this observation. Recently, Molinari and Ravichandran (2004) revisited this analysis following the constitutive framework of Clifton (1971).

The models of shock structure that are mentioned above are ultimately phenomenological and assume that the material is homogeneous. However, most experiments are conducted on polycrystalline media. One would have significant scattering and dispersion of the elastic and inelastic waves in such a media. Grady (1998) explored the scattering of waves in solids as an alternative explanation to the structured shock waves. In this analysis, elastic modes which were treated using a quasi-harmonic approximation and statistical mechanics were coupled to a nonlinear wave propagation problem. It was shown that this theory produced results in accordance with the single shock data for metals. However, the proposed model was not able to predict more complicated loading like two step shocks. A complete discussion on the fourth power law is presented by Grady (2010).

Structured shocks have also been examined in strongly heterogeneous media, and they do not display the fourth power law in general (Grady, 2010). Zhuang et al. (2003) observed a second power law in periodically layered composites. This work also highlighted the role of scattering by using stress sensors interior to the specimen. Vogler et al. (2012) reinterpreted the observations and suggested an exponent of 2.4 (instead of 2). They also found an exponent of 2–3 in particulate composites and linear relation in granular media. These different exponents in composites are attributed to the scattering of shock waves (as opposed to elastic waves).

The scattering of elastic waves (in linear media) has been widely studied both experimentally and theoretically. Much is known about periodic media where resonances create a highly frequency dependent response through the use of the Bloch–Floquet theory (Sun et al., 1968; Lee and Yang, 1973; Nayfeh, 1995). There is also an understanding of random media and how multiple scattering leads to diffusive response (Ryzhik et al., 1995).

* Corresponding author.
E-mail address: bhatta@caltech.edu (K. Bhattacharya).

http://dx.doi.org/10.1016/j.ijsolstr.2014.06.021
0020-7683/

In contrast, much less is known about nonlinear wave propagation in heterogeneous solids. Chen et al. (2004) adapted the Bloch–Floquet analysis to study plate impact on a periodically layered medium. They developed an analytic solution for the linear case, and used it to obtain an approximate solution for the nonlinear case by making an ansatz about the wave reflections and matching the impedence to nonlinear response. There is also an extensive study of interactions at individual interfaces (Davison, 2008, ch. 9) considering characteristic solutions and Riemann invariants. Since the system also contains rarefaction waves, the interaction happens over a zone and this makes the analysis quite involved.

In this work, we build on the study of individual interactions to understand *the collective response of a heterogeneous medium with multiple interfaces*. Specifically we consider a one-dimensional piecewise homogeneous material with perfectly bonded interfaces. In a typical shock process, the loading happens along the material's Hugoniot while the unloading happens along an isentrope. This leads to a system of shocks and rarefaction waves traveling in the medium. The interaction between shocks, rarefaction waves and interfaces happen over a zone and the solutions are not piecewise uniform. To keep the problem tractable, we idealize the equation of state of each segment in a piecewise affine manner so that there are no rarefaction waves and elastic waves propagate homogeneously, and the heterogeneity is limited to shock waves. We also assume isothermal conditions for simplicity.

It is customary in the study of shock waves to specify an empirical (often linear, (Ruoff, 1967)) relation between the shock speed and particle velocity. We follow Knowles (2002) instead and specify the equation of state as a relation between stress and strain, and supplement it with a kinetic relation that relates the rate of dissipation at the shock front to the shock speed. This framework was introduced in the study of phase transitions (Abeyaratne and Knowles, 1991, 1992), but has also been shown to be useful in the study of shocks (Knowles, 2002; Niemczura and Ravi-Chandar, 2011). In our context, this framework allows us to quickly identify parameters that simplify rarefaction waves and make the elastic waves propagate homogeneously.

We also neglect the structure of the shock, and treat it as a discontinuity. It is known (Abeyaratne and Knowles, 1992) that the kinetic relation can be chosen such that the dissipation at the discontinuity is exactly equal to that of the dissipation in structured shocks. It has also been recently shown (Tan and Bhattacharya, in preparation) that the equivalent sharp discontinuity treatment is appropriate when the length-scale of the heterogeneous media is large compared to the inherent length-scale of the structure shock.

There are a number of powerful numerical methods that can be used in the study of shock waves in one and higher dimensions for detailed empirical material models (see for example Zukas, 2004). These can be used to gain detailed information in specific examples. Our approach using an idealized model is unable to provide such high fidelity information. Instead, the simplified framework that we propose can provide important insight and understanding about a broad range of phenomena. Further, every numerical method has limited resolution (even if it is extremely fine), and this becomes an issue when one has multiple interfaces and reflections. Our results can be used to benchmark these numerical studies.

After recalling the governing equations in Section 3, we study the interaction between a shock wave and an interface in Section 4. Since there are no rarefaction waves, solutions are piecewise uniform in space–time and the interaction leads to a Riemann problem. We are able to solve this Riemann problem analytically. We show that increasing compressibility dissipates the shock while decreasing compressibility intensifies the shock. We extend the analysis to semi-infinite media in Section 5. We show that the shock speed and state of stress in any segment depends only on the properties of the first and that segment.

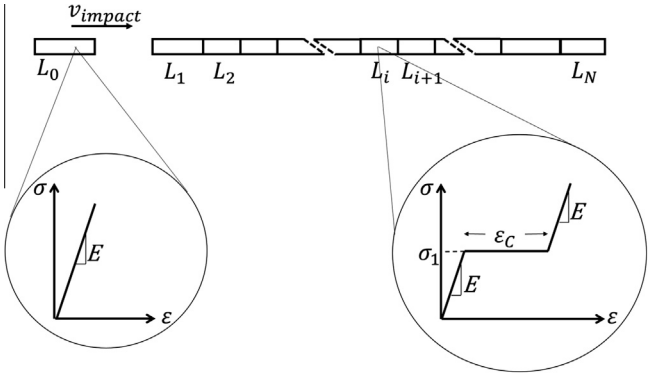

Fig. 1. Schematic representation of the impact problem.

We turn to the impact of a finite medium in Section 6. We take advantage of the fact that the solution is piecewise constant, and thus it only remains to follow the shock and elastic waves. We propose a new object oriented algorithm to solve this problem exactly. In short, we follow each (elastic and shock) wave and account for all interactions explicitly. We use this method in Section 7 to study the influence of parameters like number of interfaces, arrangement of layers in the target and length of the impactor on the dynamics of the problem on particle velocity profiles, shock structure and effective shock velocities. We use it to provide insights into the optimal arrangement for enhanced attenuation. We conclude in Section 8 with a discussion of the main results.

2. Problem statement

We analyze a plate impact induced shock propagation through an idealized nonlinear heterogeneous material. Fig. 1 provides a schematic illustration of the problem. We use the sign convention that compression is positive. We have a linearly elastic impactor traveling at the speed v_{impact} hit a heterogeneous medium or target. The right edge of the ensemble and the left edge of the impactor are free, and the impactor is free to separate from the target.

The heterogeneous medium or target is made of N segments or elements. All the interfaces are perfectly bonded. Each element is made up of a material that follows a piecewise affine stress - strain curve as shown in Fig. 1.[1] Real materials have an effective stress–strain curve that is characterized by an elastic linear region, followed by an yield or Hugoniot elastic limit, and in turn followed by a convex increasing stiffening nonlinear response (Marsh, 1980). We idealize this behavior using a piecewise affine curve. This allows the problem to be simple enough for detailed analysis while retaining the essential features like wave–wave and wave-boundary interactions. Specifically, it collapses rarefaction waves on to unloading shocks. A further idealization is that each material has the same yield strength (σ_1), Young's modulus (E) and density (ρ). So the material is elastically homogeneous. However, each material has a different compressibility ε_c and thus material is heterogeneous with respect to shock waves.

We assume for simplicity that the problem is isothermal.

3. Governing equations

We work in a Lagrangian setting. We denote particle velocity, strain and stress at the particle X in the reference configuration

[1] It is customary in the study of shocks to specify the constitutive relation as a (often linear) relation between the shock speed and particle velocity. We report this relation later for our material.

at time t to be $v(X,t), \varepsilon(X,t)$ and $\sigma(X,t)$ respectively. We assume that the system is governed by the usual compatibility and momentum balance equations. Note that we do not need an energy balance due to our isothermal assumption. Further, in light of our piecewise affine constitutive assumption as well as the nature of the impact problem, all solutions to these equations are going to be piecewise constant in the $X-t$ plane. Therefore, the governing equations reduce to the following jump conditions (Davison, 2008, ch. 2):

$$[\![\sigma]\!] + \rho \dot{s} [\![v]\!] = 0, \tag{1}$$

$$[\![v]\!] + \dot{s} [\![\varepsilon]\!] = 0, \tag{2}$$

where $\dot{s}$ is the propagation velocity of the wave or discontinuity.

We describe as an *elastic wave* a propagating discontinuity where the states on both sides of the discontinuity lie on the same branch of the stress–strain curve (e.g., from point 1 to point 2 or from point 3 to point Q in Fig. 2(a)). We describe as a *shock wave* a propagating discontinuity where the states on the two sides of the discontinuity lie on two different branches of the stress–strain curve (e.g., from point 2 to 3 in Fig. 2(a)).

For an elastic wave, it is easily shown that the two equations hold simultaneously if and only if

$$\dot{s} = \pm c := \pm\sqrt{E/\rho}. \tag{3}$$

Further, for this wave speed, the two equations above become degenerate.

For a shock, the equations above are insufficient to prove a unique propagation speed. Typically, an empirical linear relation between shock velocity and particle velocity is used (Asay and Shahinpoor, 1993; Davison, 2008; Meyers, 1994) to deal with this non-uniqueness. Here, we instead follow Knowles (2002) and specify a *kinetic relation* or *entropy condition*. It is easily shown that the rate of dissipation or rate of entropy production at a propagating shock is given by the product of the shock speed and the driving force which is the signed area between the stress–strain curve and the line joining the two states (the difference in areas enclosed by triangle $3PQ$ and triangle $12P$ in Fig. 2(a)). The kinetic relation or entropy condition is an empirical relation between the rate of dissipation and the shock speed.

We specifically assume the *maximally dissipative* kinetic relation that maximizes dissipation amongst all possible admissible shocks (Knowles, 2008). Thus, for a shock which takes a state on the low-strain branch to a state on high-strain branch, the maximum dissipation is attained when the low strain state is at point 1 in Fig. 2(a). Similarly, for a shock which takes a state on the high-strain branch to a state on low-strain branch, the maximum dissipation is attained when the low strain state is at point Q in Fig. 2(a). Thus,

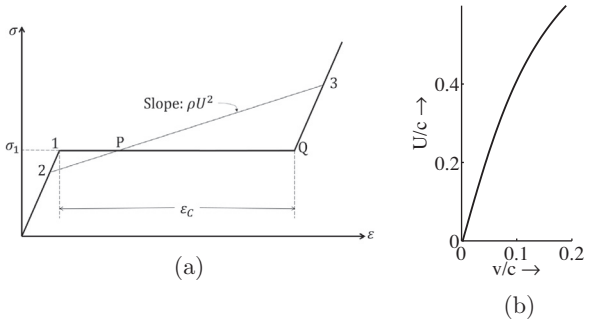

Fig. 2. (a) Illustration of a possible shock wave that satisfies balance laws on $\sigma-\varepsilon$ plane. A maximally dissipative loading shock always starts from 1 while a maximally dissipative unloading shock always starts from Q. (b) Shock speed vs. particle velocity jump for a maximally dissipative loading shock.

the maximally dissipative kinetic law states that admissible shocks are limited to the following:

- Loading: shocks loading from low strain branch to high strain branch start at state 1;
- Unloading: shocks unloading from high strain branch to low strain branch start at state Q.

We conclude this section by observing that the formulation above is equivalent to one that specifies a relation between the shock speed and (jump in) particle velocity. Notice that for our stress–strain curve, we have

$$[\![\sigma]\!] = E([\![\varepsilon]\!] - \varepsilon_c). \tag{4}$$

We can use this and the jump conditions (1) and (2) to eliminate $[\![\sigma]\!]$ and $[\![\varepsilon]\!]$ and obtain a relation between the shock speek $\dot{s} = U$ and the (jump) in particle velocity.

$$-[\![v]\!] = \frac{Uc^2\varepsilon_c}{c^2 - U^2}. \tag{5}$$

While this is not linear, it can be approximated by one for a large range of under-driven shocks as shown in Fig. 2(b).

4. Interaction of a shock wave and a material interface

We begin with a simple problem that reveals the behavior of shocks at the interface between two elements. We consider two materials A and B with an interface separating them. They are initially stress free and a stress $\sigma_0 > \sigma_1$ is imposed on the left side of material A. The $X-t$ diagram of the process is presented in Fig. 3(a) with the particle velocity and stress constant in each region. An elastic wave and a shock wave originate at the origin and travel into material A. The elastic wave travels faster than the shock-wave, and proceeds unimpeded into material B due to our constitutive assumption of uniform modulus and density. It follows from maximally dissipative kinetics that the elastic wave takes both material A and B to state 1 corresponding to the point 1 in Fig. 3(b). The shock wave that follows takes material A from state 1 to state 2 shown in Fig. 3(b) with $\sigma_2 = \sigma_0$. The jump conditions across the elastic wave and the shock wave is given by

$$\sigma_1 - 0 + \rho c(v_1 - 0) = 0, \tag{6}$$

$$\sigma_2 - \sigma_1 + \rho U_A(v_2 - v_1) = 0, \tag{7}$$

$$v_2 - v_1 + U_A(\varepsilon_2 - \varepsilon_1) = 0. \tag{8}$$

Since $\sigma_1, \varepsilon_1, \sigma_2, \varepsilon_2$ are known, we solve these equations to obtain v_1, v_2, U_A to be

$$v_1 = -\frac{\sigma_1}{\rho c}, \tag{9}$$

$$U_A = \sqrt{\frac{\sigma_2 - \sigma_1}{\rho(\varepsilon_2 - \varepsilon_1)}}, \tag{10}$$

$$v_2 = v_1 - \sqrt{\rho(\sigma_2 - \sigma_1)(\varepsilon_2 - \varepsilon_1)}. \tag{11}$$

As soon as the shock traveling in material A hits the interface, three things can potentially happen:

1. A backward propagating elastic wave appears in material A taking it to point 3.
2. A forward propagating elastic wave in material B taking the material from point 1 to point 4.
3. A forward propagating shock wave in material B taking it from point 4 to point 5.

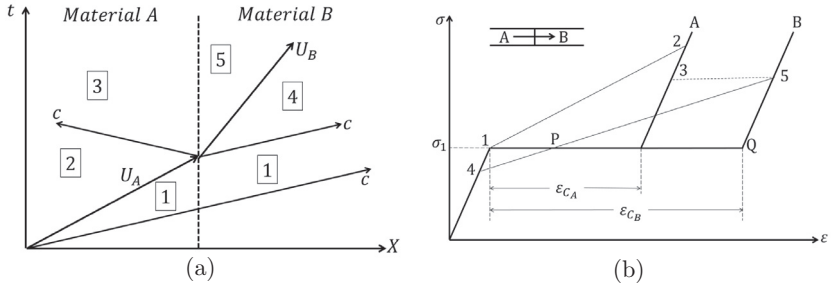

Fig. 3. (a) X-t diagram of the shock interaction process. (b) Representation of the stress states on the stress–strain curve.

However, according to the maximally dissipative kinetics applied to material B, state 4 has to equal state 1.[2] Thus, we do not have a forward propagating elastic wave in material B. Further, since the interface is perfectly bonded, states 3 and 5 are equal ($\sigma_3 = \sigma_5, v_3 = v_5$). Thus, it only remains to compute state 3 as well as the shock wave U_B. We do so by solving the remaining jump conditions – one across the backward elastic wave in material A and two across the shock wave in material B:

$$\sigma_3 - \sigma_2 - \rho c(v_3 - v_2) = 0, \tag{12}$$

$$\sigma_3 - \sigma_1 + \rho U_B(v_3 - v_1) = 0, \tag{13}$$

$$v_3 - v_1 + U_B(\varepsilon_3 - \varepsilon_1) = 0. \tag{14}$$

We can solve these for the remaining unknowns σ_3, v_3, U_B noting that σ_3 and ε_3 are related through the stress–strain curve. We obtain

$$\sigma_3 = \frac{E\varepsilon_c^B\sigma_1 - \sigma_1^2 + (\sigma_2 + \rho c(v_1 - v_2))^2}{2(\sigma_2 - \sigma_1) + \rho c(\varepsilon_c^B c + 2v_1 - 2v_2)}, \tag{15}$$

$$v_3 = \frac{(E\varepsilon_c^B(\sigma_1 - \sigma_2 + \rho c v_2)) - (\sigma_1 - \sigma_2 + \rho c(-v_1 + v_2))(\sigma_1 - \sigma_2 + \rho c(v_1 + v_2))}{\rho c(-2\sigma_1 + 2\sigma_2 + \rho c(\varepsilon_c^B c + 2v_1 - 2v_2))}, \tag{16}$$

$$U_B = \frac{\sigma_2 - \sigma_1 + \rho c(v_1 - v_2)}{\sigma_2 - \sigma_1 + \rho c(\varepsilon_c^B c + v_1 - v_2)} c. \tag{17}$$

It follows from the equations above that

$$U_B = \frac{rU_A c}{c + (r-1)U_A}, \tag{18}$$

where

$$r = \frac{\varepsilon_c^A}{\varepsilon_c^B}$$

may be regarded as a compliance ratio.

A few comments are in order. First, we see from (18) that $U_B = U_A$ if $r = 1$ and that $dU_B/dr < 0$. Therefore, we conclude that if the compliance ratio $r < 1$ so that the shock passes from a stiff material to a compliant material, the shock speed decreases and vice versa. Further, it follows from Fig. 3(b) that the stress follows the same trend: stresses decrease when the shock passes from a stiff material to a compliant one, and vice versa. We can not obtain an expression for σ_3 in terms of r (as in (18)) because ε_c terms can not be eliminated completely from (15).

Second, no forward moving elastic wave is generated when the shock wave interacts with the material interface. This is independent of the compliance ratio. This will prove important in future discussion. Third, notice that the backward moving elastic wave eventually brings the entire element to the stress state σ_5. Finally, if the compliance ratio $r < 1$, then the backward moving elastic wave unloads the material, and vice versa. In a realistic material where the Hugoniot is curved, the interaction of the shock wave at the interface depends on the impedance ratio ($Z = \rho_A C_0^A/\rho_B C_0^B$) of the two materials involved. Here C_0^i is the initial sonic velocity of the material *i*. The problem is described in Davison (2008, ch. 3 and 9) and Meyers (1994, ch. 7). We consider the case where $Z < 1$. In this case, the shock upon interaction, produces two shock waves propagating into material A and B. In our model, this is equivalent to the case when $r > 1$ where we see a loading elastic wave traveling back into the material A. For $Z > 1$, the interaction results in a shock wave in *B* and a rarefaction fan in material *A*. This is equivalent to $r < 1$ in our case where an elastic wave of unloading nature propagates in *A*. There are no fans here due to the particular choice of constitutive relation.

5. Shock wave propagation in a semi-infinite medium

We now turn to the heterogeneous material shown in Fig. 1 with multiple segments. As a first step, we assume that the impactor and last element of the ensemble are semi-infinite. This assumption means that no elastic waves reflect from the free ends and interact with the advancing shock wave. Further, recall from the earlier section that no forward moving elastic wave is generated when the shock interacts with the interface. Together, these means that the shock wave never interacts with an elastic wave as it passes through the medium and that the interaction of the shock wave with each interface is exactly as described in the previous section. Therefore, we can obtain a solution by a sequence of solutions to the single interface problem. So the shock speed at the *N*th element can be calculated by recursively applying (18). We conclude

$$U_N = \frac{r_N U_1 c}{c + (r_N - 1)U_1}, \tag{19}$$

where $r_N = \frac{\varepsilon_c^1}{\varepsilon_c^N}$ is the compliance ratio of the first and last elements.

This means that the shock speed at the *N*th element depends only upon the incident shock speed and the properties of first and last element. The arrangement of intermediate materials does not matter. From (19), it can be observed that $U_N < U_1$ (and hence $\sigma_N < \sigma_1$) if $\varepsilon_c^N > \varepsilon_c^1$. As before, this follows the same trend. Stresses and particle velocity at the *N*th element are also independent of the arrangement of the intermediate elements. Again, it must be noted that the receding elastic waves will cause the entire ensemble to eventually reach σ_N stress state.

[2] Precisely $\sigma_4 = \sigma_1$ and then the jump condition implies that $v_4 = v_1$.

6. Impact of a finite heterogeneous medium: method

We are now in a position to consider the problem shown in Fig. 1. This is considerably more difficult than the problems considered above because the elastic waves reflect off the free end and interact with the shock. So we have to proceed numerically. We take advantage of the fact that the solution (v, σ) is piecewise constant in the $X-t$ plane, and thus it only remains to follow the waves. Our numerical method follows each elastic or shock wave as it is nucleates, propagates, reflects and otherwise interacts with other waves. As a first step towards this, we catalog all possible interactions between waves, interfaces and free-ends. Note that each of these may be posed (locally in $X-t$) as a Riemann problem with piecewise constant initial data at the instant of interaction.

6.1. Individual interactions

We begin by cataloging all possible interactions and the associated Riemann problems:

1. Reflection of elastic wave from a free edge.
2. Elastic wave interacting with another elastic wave.
   (a) Interaction in a linearly elastic medium.
   (b) Interaction in a piecewise affine medium.
      i. Interaction of elastic waves resulting in the formation of two elastic waves.
      ii. Interaction of elastic waves in low strain branch forming a compression shock pair.
      iii. Interaction of elastic waves in high strain branch forming an unloading shock pair.
   (c) Interaction at the interface of linear and piecewise affine medium.
      i. Formation of two elastic waves.
      ii. Formation of a compression shock in the piecewise affine layer.
      iii. Formation of an unloading shock in the piecewise affine layer.
3. Elastic wave from piecewise affine material interacting with material boundary.
4. Elastic wave from a purely elastic medium entering a piecewise affine medium.
   (a) Elastic wave of high compression amplitude leads to a compression shock.
   (b) High amplitude elastic wave of tensile nature leads to an unloading shock.
   (c) Elastic wave of sufficiently low amplitude passes through unaffected.
5. Compression shock interacting with an interface.
   (a) Interface joining a linearly elastic and a piecewise affine layer.
   (b) Interface connecting two piecewise affine layers.
6. Unloading shock interacting with an interface.
   (a) Interface joining a linearly elastic and a piecewise affine layer.
   (b) Interface connecting two piecewise affine layers.
7. Elastic wave interaction with a shock wave.
   (a) Interaction with a compression shock traveling in the same direction.
   (b) Interaction with a compression shock traveling in opposite direction.
   (c) Interaction with an unloading shock traveling in the same direction.
   (d) Interaction with an unloading shock traveling in opposite direction.
8. Interaction of two shock waves traveling in opposite direction.
   (a) Interaction of two compression shocks.
   (b) Interaction of two unloading shocks.

We find explicit solutions to each of these problems following the method in Section 4. These are listed in Appendix A.

6.2. Numerical method

Our numerical method follows all the waves in the system. We treat each wave as an *object* that contains origin and endpoints in the $X-t$ plane, the speed, the direction, the state (σ, ε, v) before and after the wave, the material in which it is propagating and the *status* of the wave. At any instant of time, the status of each wave that is propagating in the system is *active* while that of the others is *inactive*. We then find the smallest time when any of the active waves interact with another active wave or interface or boundary. We then look up the solution to the appropriate Riemann problem, update the list of waves (reclassify as active/inactive or introduce new waves if necessary) and proceed. We have implemented this in MATLAB.

Notice that this numerical method produces the *exact* solution as there is no discretization of either time or space. The only possible source of errors are the round-off errors in computing the time of interaction and the explicit solution of the Riemann problems.

7. Impact of a finite heterogeneous medium: results

All calculations are performed for the following parameters: $\rho = 2700\ \text{kg/m}^3$, $c = 6000\ \text{m/s}$, $\sigma_1 = 200\ \text{MPa}$, $E = \rho c^2$, $v_{impact} = 1000\ \text{m/s}$, length of target bar 1 m. The following parameters are varied from simulation to simulation: length of the impactor L_0, number of segments N and profile of the plateau strain ε_c (though the range is always from 0.2 to 0.6). The range of ε_c is to chosen for both demonstrative purposes and to keep the relation between the shock speed and the particle velocity in the linear regime shown in Fig. 2(b). The analysis holds true smaller values of ε_c. The length of all segments are equal so that their length is $1/N$.

7.1. Typical results

A typical result is shown in Fig. 4(a). This simulation has $L_0 = 1\ \text{m}, N = 20$ and ε_c decreasing linearly from 0.6 to 0.2 along the length of the target. The impactor is represented by the region $X \in [0, 1]m$. As mentioned before, the left edge of the impactor ($X = 0$ m) and the right edge of the ensemble ($X = 2$ m) are free. The impactor is free to separate from the target. However, this phenomenon is not observed during this simulation. The vertical lines represent the element boundaries. The (narrow) red lines are the elastic waves while the (bold) black lines are the shock waves.

At the moment of impact ($t = 0$), we see compressive elastic waves moving into the impactor and the target followed by a shock wave in the target. As per our assumption, the target is homogeneous to elastic waves. Hence, the elastic waves travel through the target unimpeded. The compression shock, on the other hand, interacts with the interfaces setting off backwards propagating elastic wave at each interface. Since ε_c decreases (the effective stiffness increases) along the length, the shock speed increases (by (18)) and the backwards propagating elastic wave further loads the material. The leading elastic waves in the target and the impactor eventually reach the free end and reflect back as tensile (unloading) elastic wave. The reflected elastic wave (of unloading

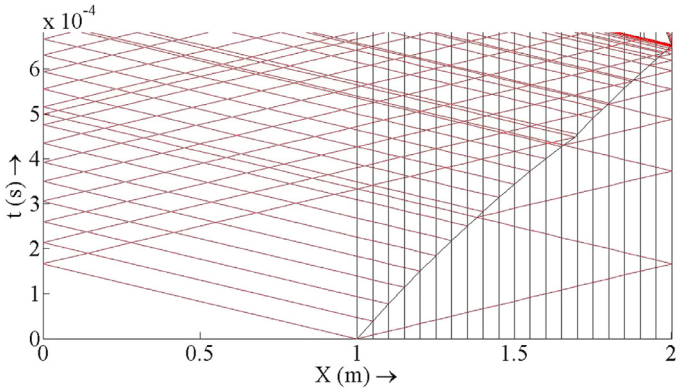

(a) $X - t$ diagram

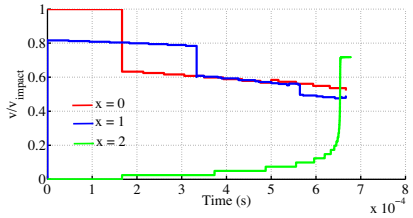

(b) Particle velocity plot at $X = 0m$ (left edge of impactor), $X = 1m$ (interface) and $X = 2m$ (right edge of the ensemble)

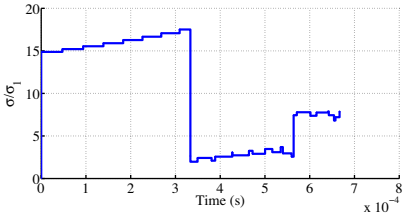

(c) Stress profile at $X = 1m$

Fig. 4. Impact problem for $L_0 = 1$ m and ε_c decreasing linearly.

nature) in the target interacts with the shock wave as shown. This interaction leads to formation of new elastic waves which in turn reflect back and interact with the shock. This kind of interaction happens over and over again until the compression shock changes its direction and nature. In other words, the interaction of type 7(b) happens over and over again until the solution shown in Fig. 21(b) dominates over the one in Fig. 21(c). It is important to note that the shock never actually reaches the free edge. The reflection of compression shock as a tensile shock happens very close (but just before) to the free edge of the target. Meanwhile in the impactor, the reflected elastic wave (of unloading nature) interacts with a series of backwards propagating elastic waves (of loading nature) before interacting with the shock.

Particle velocities measured by velocity interferometry (VISAR) or Doppler velocimetry (PDV) are often the only way of interrogating shock waves in experiment and provide valuable insights into the rise times and peak pressures achieved in the target. A summary of most commonly used experimental methods can be found in Asay and Shahinpoor (1993). Fig. 4(b) shows the particle velocity profiles at $X = 0$ m (left end of the impactor), $X = 1$ (the point of impact) and $X = 2$ (the right edge of the ensemble) for the result shown in Fig. 4(a). An important observation of the particle velocity profile at the free (right) end of the impactor ($X = 2$) is that the heterogeneities does not give rise to a structured shock. We see a series of elastic precursors followed by a sharp rise or spike corresponding to the time compression shock reflects off as unloading shock. We see this repeatedly in our simulations and is consistent with some recent experimental observations (Rauls and Ravichandran, in preparation). Fig. 4(c) shows the variation of stress at the point of impact ($X = 1$) for this case. The sharp decline observed at $t \sim 3.3 \times 10^{-4}$ s corresponds to the time when first release wave from the impactor hits the impactor/target interface.

Similar results are presented for ε_c increasing case in Fig. 5(a)–(c). For ε_c increasing case $\varepsilon_c^1 = 0.2$, while for ε_c decreasing case, $\varepsilon_c^1 = 0.6$. Hence for the same impact speed, initial shock speed (and hence stress) is higher in ε_c increasing case. This explains the difference in stresses at $t = 0$ in Figs. 4(c) and 5(c). Further, the receding elastic waves, formed by the interaction of shock wave with layer interfaces, are of unloading nature. Hence the unloading nature of the release waves is intensified. At $t \sim 3.3 \times 10^{-4}$ when release wave hits the impactor/target interface, the impactor separates. This is observed in the Fig. 5(c) when the stress becomes zero. As this release wave goes further into the target, it interacts with more receding elastic waves leading to the formation of pairs of unloading shocks (interaction of type 2(b).iii). Under certain conditions like higher impact speeds or higher contrast in the target, tensile stresses develop within these pairs corresponding to the possibility of spallation. This will be studied in detail in Section 7.4.

7.2. Effect of reflected waves

7.2.1. Shock arrival times

The shock arrival time is the time taken by the compression shock wave to the reach the free edge of the target before reflecting off as an unloading shock wave. Since the wave never fully reaches the free end as discussed above, we define this time T as the time where the compression shock wave reverses direction. Fig. 6 shows the plot of shock arrival time T vs the number of elements N in the ensemble for the case $L_0 = 5$ m. Since $L_0 = 5$ m, the release waves from the impactor do not reach the shock front. The effect of release will be studied separately. The figure also shows the shock arrival time at 1 m for a semi-infinite medium (no reflections) studied earlier. Note that for the semi-infinite case, the arrival times are independent of number of interfaces and ε_c profiles. This is because the ε_c profiles are chosen linear and the layers have identical thickness. This will not hold in general. The reflected elastic waves have two effects on the shock waves. First, it slows down the shock wave in both cases. This is because the reflected waves are unloading in nature. Second, it breaks the symmetry: the point of interaction in the target becomes important as the shock wave is

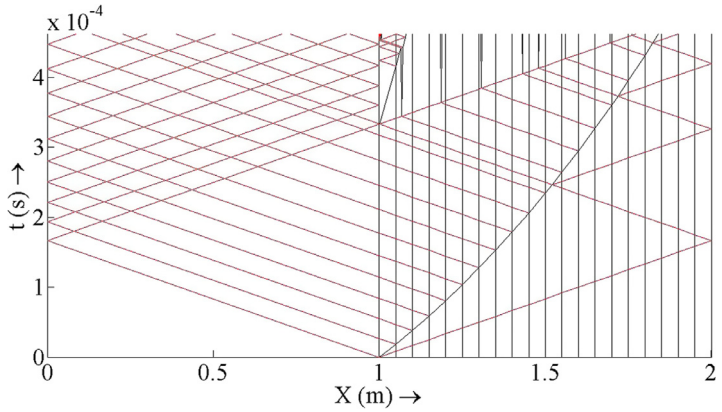

(a) $X - t$ diagram

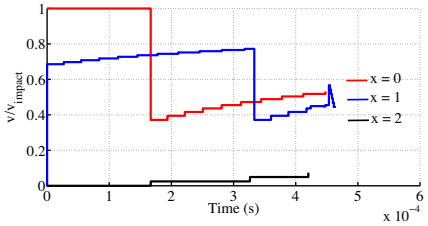

(b) Particle velocity plot at $X = 0m$ (left edge of impactor), $X = 1m$ (interface) and $X = 2m$ (right edge of the ensemble)

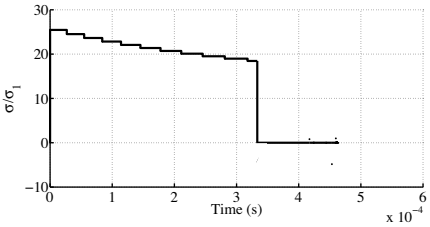

(c) Stress profile at $X = 1m$

Fig. 5. Impact problem for $L_0 = 1$ m and ε_c increasing linearly.

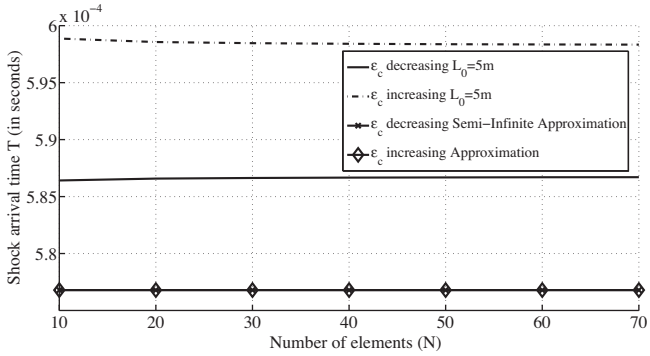

Fig. 6. Plot of shock arrival time T vs N.

slower in the material with increasing ε_c (progressively more complaint).

7.2.2. Number of elements

Fig. 6 shows that the number of segments have only a marginal effect on shock velocity.

Fig. 7(a) and (b). compares the particle velocity profiles (normalized by impact velocity) for different values of *N*. For comparison, calculations were also performed for the case when all the elements have the same value of ε_c. In every simulation the total length of the ensemble is kept constant. Once again, it is observed that *N* does not have a significant influence over the particle velocity profiles. The profiles overlap and are bounded by the homogeneous cases of $\varepsilon_c = 0.2$ and $\varepsilon_c = 0.6$. In accordance with Fig. 6, the arrival times remain fairly constant with *N*. The slow decrease (increase) observed in ε_c increasing (decreasing) case in the post shock phase is the result of the elastic waves between the free edge and the reflected unloading shock.

7.2.3. Alternating linear and nonlinear material

In order to further understand the significance of reflected elastic waves, we study a different type of target. Given *N* (even), we construct a target of $N - 1$ layers such that every alternate layer (total of $N/2 - 1$ layers) is purely elastic and remaining $N/2$ layers are elastic plastic with identical values of ε_c. The layers have identical length while the total length of the target is 1 m. The calculations were performed for various values of *N* for $\varepsilon_c = 0.2$ and 0.6. Fig. 6(a) and (b) show the particle velocity profiles at the free end of the target.

Unlike in Fig. 7(a) and (b), the particle velocity profiles vary with *N* in Fig. 6(a) and (b). The reflected elastic wave can interact with either elastic wave in the elastic layer (interaction of type 2 in Section 6.1) or the shock wave in the piecewise affine layer (interaction of type 7(b) in Section 6.1). This leads to different evolution of shock profile as *N* changes. From Fig. 8(a) and (b), we can see that the arrival times decrease as *N* increases. This is particularly interesting because the total length of the elastic layers is same for all *N*. This effect is purely due to the different interactions of reflected waves. The decrease in arrival times imply that the effective shock speed is increasing with *N*. In the case of $\varepsilon_c = 0.6$, the shock speed in the system is slower than that in $\varepsilon_c = 0.2$ case which accounts for the difference in arrival times.

The decrease observed in the particle velocity profiles after the peak is achieved is due to the tensile shock hitting the elastic layer on the way back. The magnitude of this decrease is independent of *N* because the Riemann problem remains independent of the thickness of the layers. There is an increase when the next piecewise linear layer is encountered followed by another decrease at the next elastic layer. These oscillations continue until either the release wave enters the target or the tensile shock hits the target/impactor interface. The period of oscillation is determined by the thickness of the layers and number of interfaces in the target. This is consistent with the analysis in Chen et al. (2004) and Chen and Chandra (2004).

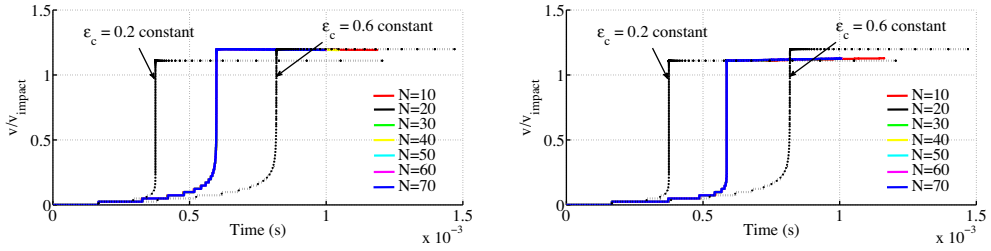

(a) ε_c increasing (b) ε_c decreasing

Fig. 7. Variation of particle velocity plots with N for $L_0 = 5$ m.

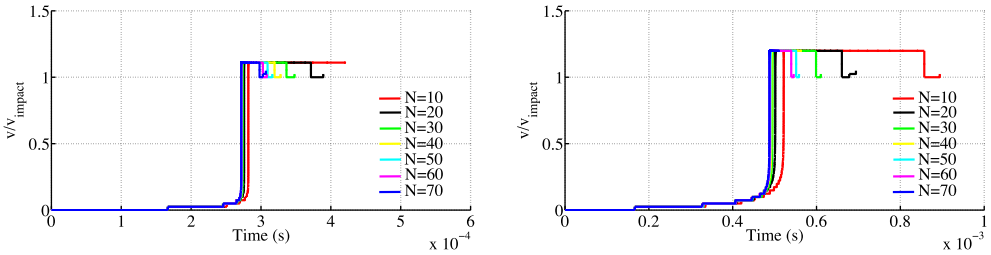

(a) $\varepsilon_c = 0.2$ constant (b) $\varepsilon_c = 0.6$ constant

Fig. 8. Variation of particle velocity profiles with N for alternate elastic and piecewise affine layered target for $L_0 = 5$ m.

7.3. Effect of ε_c profiles

In Sections 7.2.1 and 7.2.2, we considered a linear variation in the value of ε_c along the length of the ensemble. We now study other variations. Through out this section, we take the impactor length to be very long $L_0 = 5$m so that we do not encounter a release wave.

7.3.1. Power law profile

We consider a power law variation of ε_c along the length of the target between the values 0.2 and 0.6. Specifically, we assume that

$$\varepsilon_c^i = a + b\left(\frac{i-1}{N-1}\right)^n, \quad i = 1, \ldots, N, \tag{20}$$

where $a = 0.2, b = 0.4$ for the increasing case and $a = 0.6, b = -0.4$ for the decreasing case. We take $N = 20$. We study the particle velocity profiles for linear, quadratic, cubic and quartic exponents ($n = 1, \ldots, 4$). The particle velocities at end of the target are shown in Fig. 9(a) and (b). We see that the shock arrival times decreases with n in Fig. 9(a) while it increases in Fig. 9(b). We understand this by recalling from our analysis in Section 4, that the shock slows down if ε_c increases across the interface. As n increases, the increase in ε_c is slower in the beginning of the ensemble.

7.3.2. Step ε_c profiles

Next we consider a step profile for ε_c along the length of the ensemble. We assume that ε_c takes one value (0.2 for increasing and 0.6 for decreasing) in $[0, \lambda)$ and another (0.6 for increasing and 0.2 for decreasing) in $[\lambda, 1]$. The particle velocities at the end of the target are shown in Fig. 10(a) and (b) for various values of λ. For comparison, particle velocity profiles for $\varepsilon_c = 0.2$ and 0.6 constant (ref: Fig. 7(a)) are also shown. For the increasing case (Fig. 10(a)), the arrival time decreases with increasing λ since it travels larger distances in the stiffer $\varepsilon_c = 0.2$ material. The opposite is true for the decreasing case (Fig. 10(b)). Notice that in both cases, profiles corresponding to constant ε_c bound the λ–dependent profiles.

7.3.3. Alternating material

In order to further understand the role of ε_c in the problem, we consider a target with alternate arrangement of $\varepsilon_c = 0.2$ and $\varepsilon_c = 0.6$ layers. The particle velocity profiles at the free edge of the target are shown in Fig. 11(a) and (b). Notice that unlike Fig. 8(a) and (b), N plays almost no role in this case till the peak ratio of v/v_{impact} is achieved. In Fig. 8(a) and (b), the reflected elastic wave was interacting with either shock wave (in a piecewise affine medium) or an elastic wave (in a purely linear medium). In that case, the particle velocity profile changed drastically

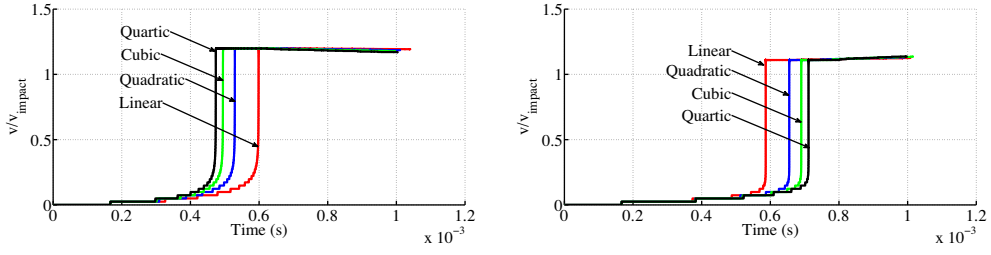

(a) ε_c increasing (b) ε_c decreasing

Fig. 9. Variation of particle velocity profiles with ε_c exponent for $L_0 = 5$ m.

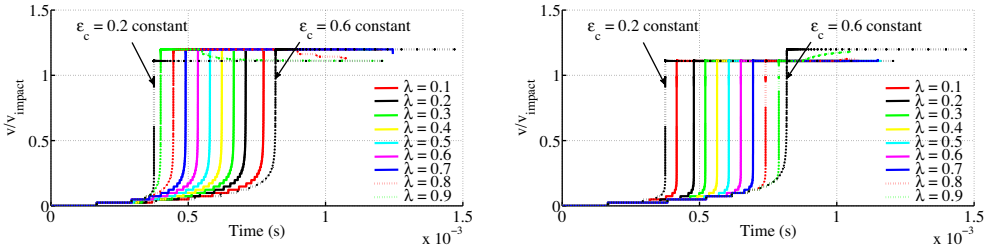

(a) ε_c increasing (b) ε_c decreasing

Fig. 10. Variation of particle velocity profiles with λ for $L_0 = 5$ m.

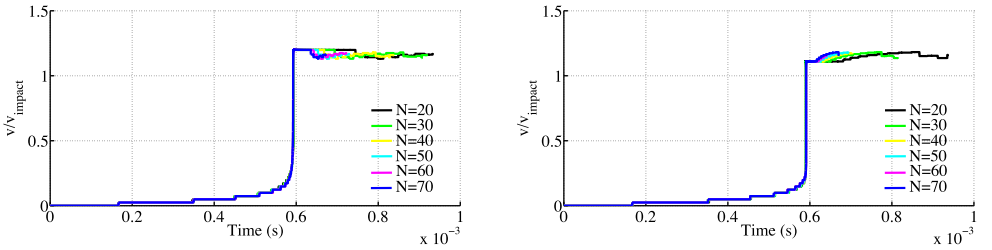

(a) Alternate $\varepsilon_c = 0.2$ and $\varepsilon_c = 0.6$ layers (b) Alternate $\varepsilon_c = 0.6$ and $\varepsilon_c = 0.2$ layers

Fig. 11. Variation of particle velocity profiles with N for alternate $\varepsilon_c = 0.2$ and $\varepsilon_c = 0.6$ layered target for $L_0 = 5$ m.

(marginally) when the reflected elastic wave interacted with an elastic (shock) wave. We also take a hint from our results in Fig. 7(a) and (b) where the particle velocity profiles were (almost) independent of N.

In this case, the reflected elastic wave interacts with either a slow propagating shock (in $\varepsilon_c = 0.6$ layer) or a fast propagating shock (in $\varepsilon_c = 0.2$ layer). In both cases the particle velocity profiles only change marginally. This explains why the profiles overlap in Fig. 11(a) and (b) till the arrival time. N starts to play a role after the compression shock reflects off the free edge as an unloading shock. We observe small oscillations in the particle velocity profiles after the reflection. These correspond to the interaction of unloading shock at material interfaces on its way back. The argument is similar to the one presented in Section 7.2.3.

7.4. Effect of release waves

The impact initiates compressive elastic waves in the impactor (see Fig. 4(a)) which is then reflected from the free boundary (release wave). These waves are of unloading nature. Since the elastic wave speed is always greater than the shock speed, the release wave eventually catches up with the shock front. Till now, we avoided this interaction by taking a long impactor, $L_0 = 5$ m. We now include this interaction by taking $L_0 = 0.5$ m.

In a heterogeneous target, the release waves interact with the receding elastic waves from the interfaces before interacting with the shock wave. These receding waves can either be of loading or unloading nature depending on the compliance ratio of the layers in the target. As a result, the unloading nature of the release waves can be reduced or intensified. This is evident while comparing the $X - t$ diagrams of Figs. 4(a) and 5(a). In Fig. 4(a) which corresponds to decreasing ε_c and thus increasing stiffness, the receding elastic waves are of loading nature which reduces the unloading nature of release waves. This is evident from the fact that we do not see separation between the impactor and the target. On the other hand, in Fig. 5(a) where one has increasing ε_c and thus decreasing stiffness, the unloading nature of the receding wave intensifies the release wave resulting in the separation of impactor and the target (Fig. 5(c)). Further, interaction of release waves with receding elastic waves (of unloading nature) in the target leads to the formation of a pair of unloading shocks.[3]

Fig. 12(a) and (b) show the $X - t$ diagrams of the impact process on a target with $N = 2$ and $N = 20$ layers. In both cases, the ε_c increases in equal steps from $\varepsilon_c^1 = 0.2$ in the first layer to $\varepsilon_c^N = 0.6$ in the final layer. Hence by (19) the ratio of the shock speeds and stresses in the first and last layers would be the same if we neglected the reflections from the free edge and the release. However, the contrast at the interface for the case $N = 2$ is much larger than the contrast at any of the interfaces for the case $N = 20$. Therefore, according to the analysis in Section 4, the unloading of the receding elastic wave for $N = 2$ case is stronger than any of the receding elastic waves in $N = 20$ case. This strong receding wave for $N = 2$ interacts with the release wave and can lead to negative (i.e., tensile) stresses as shown in Fig. 12(a). This in turn can *lead to spallation*. On the other hand, the stresses do not become negative for the case $N = 20$ as shown in Fig. 12(b) since the receding waves are gentler.

Spallation resulting from reflections from free edges has been extensively studied (see for example Bushman et al., 1992). Recent numerical and analytic studies of stress wave propagation in heterogeneous media have also shown that there can be significant variation in the critical stress and location of spall due to internal stress variations (Erzar et al., 2011; Vogler and Clayton, 2008; Wang et al., 2006). The example here shows that internal interfaces with high contrast can also give rise to internal receding waves which can result in spallation.

7.5. Dissipation

The shock is dissipative by nature. Since the elastic waves change the stress state of the medium along the same branch of the stress–strain curve, they do not dissipate any energy. From Fig. 2(a) the dissipation (per unit volume) due to shock U_A is the area between the stress strain curve and the line 2–3. In all the

[3] For a non-piecewise equation of state, these would be fans.

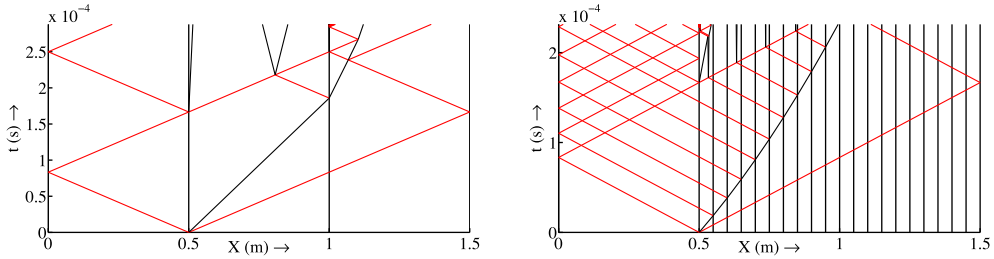

Fig. 12. $X-t$ diagrams for target with ε_c increasing and impactor length $L_0 = 0.5$ m.

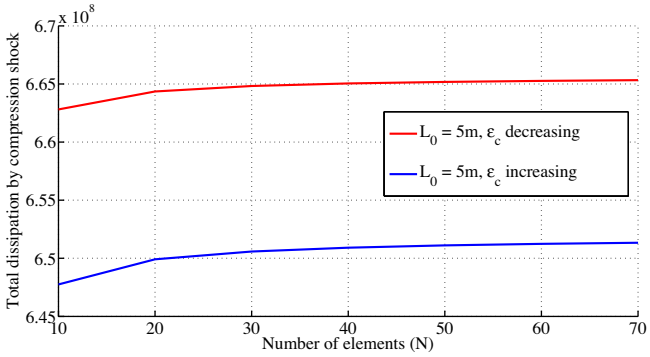

Fig. 13. Plot of total dissipation due to compression shock vs N.

Riemann problems, we assume a maximally dissipative kinetics. This is equivalent to saying that the stress state ahead of the shock wave is σ_1. Using the maximally dissipative kinetics, we can prove that point 4 in Fig. 3(b) coincides with point 1. Fig. 13 shows the total dissipation in the ensemble due to the compression shock only. The ε_c profiles chosen are linear ranging from 0.2 to 0.6 and the impact velocity $v_{impact} = 1000$ m/s. The qualitative behavior of dissipation in Fig. 13 is more important that the quantitative values.

The dissipation shows a nominal increase with N when $L_0 = 5$ m. This is because the release waves do not interact with the compressive shock and hence the dynamics is almost independent of N. This is consistent with Fig. 7(a) and (b) where the particle velocity profiles at the free edge show almost no dependence on N. Since the stress state before the compression shock is always σ_1 because of maximally dissipative kinetics, the shock speed directly corresponds to the dissipation involved. In other words, the dissipation plots can be explained using the arguments used before.

8. Conclusions and discussion

In this paper, we have studied impact problems on a one-dimensional heterogeneous medium with the goal of gaining insights into the overall shock propagation phenomenon in the presence of multiple interfaces. The propagation of shock waves in homogeneous solids has been extensively studied (Davison, 2008). The interaction of a shock with a single interface has been studied extensively in the literature (Davison, 2008, ch. 3 and 9). However, relatively less is known about the overall consequence of the interaction of a shock with multiple interfaces and this is the focus of our work.

We use the constitutive framework proposed by Knowles (2002), but show that this is consistent with the more traditional approach of specifying a relationship between the particle velocity and the shock speed. In order to focus on shock wave propagation, we considered a model situation where the medium is heterogeneous to the shock wave but homogeneous to the elastic waves and where unloading rarefaction fans collapse into unloading shocks. In light of this constitutive assumption, our solutions are always piecewise constant in the $x-t$ plane. Thus, the whole problem reduces to one of understanding interactions between various waves and interfaces. We classify all such interactions and use an object oriented program to track them and advance all the waves and shocks in time.

There are a number of powerful numerical methods that can be used in the study of shock waves in one (and higher) dimensions for detailed empirical material models (see for example Zukas (2004)). While these provide detailed information in specific examples, our idealized approach allows us to gain insight and understanding about a broad range of phenomena. Further, every numerical method has limited resolution (even if it is extremely fine), and this becomes an issue when one has multiple interfaces and reflections. Our results can be used to benchmark these numerical studies.

We investigated in some detail the problem of shock mitigation (respectively intensification) in a medium with decreasing (respectively increasing) stiffness. We found the surprising result that if we neglect all reflections as for example in a semi-infinite medium, the instantaneous shock wave speed and state of stress in the Nth element depends only on the properties of first and Nth element (Section 5). Of course the shock arrival time (or the overall shock speed) depends on the actual profile since the overall shock speed is the harmonic mean of the segment-wise shock speed. Elastic waves reflected from the free edge change the situation. Since each reflected elastic wave is unloading in nature, it slows down the shock wave. While each interaction is small, they can collectively lead to significant differences (Section 7.1).

A more important distinction is observed in a situation with a small impactor that results in a release wave (Section 7.4). This is due to the interaction between this release wave and the elastic waves from the interaction between the shock wave and the material interfaces. In particular, for a material with decreasing stiffness as would be used for shock mitigation, these interactions can lead to an unloading shock, a tensile state of stress and possible spallation. This happens when the drop in stiffness is sudden, but not when this is more gradual. Spallation resulting from reflections from free edges has been extensively studied (see for example Bushman et al. (1992)). Recent numerical and analytic studies of stress wave propagation in heterogeneous media have also shown that there can be significant variation in the critical stress and location of spall due to internal stress variations (Erzar et al., 2011; Vogler and Clayton, 2008; Wang et al., 2006). Our example shows that internal interfaces with high contrast can also give rise to internal receding waves which can also result in spallation. Further, we observe that the amount of energy dissipated increases with the number of interfaces (Section 7.5). We thus conclude that is is preferable for mitigation to have a material with many layers (graded material) than one with an abrupt change in stiffness.

A recurring observation is that heterogeneities do not necessarily lead to structured shocks. We see a series of elastic precursors followed by a sharp rise or spike corresponding to the time compression shock reflects off as unloading shock. This is consistent with some recent experimental observations (Rauls and Ravichandran, in preparation). This remains true also in materials with alternating stiffness (or alternating linear and nonlinear materials). However, in such materials, one sees an oscillation in the particle velocity at the free surface. This is consistent with observations (Zhuang et al., 2003) and previous numerical studies (Chen et al., 2004; Chen and Chandra, 2004).

Acknowledgement

We are grateful to G. Ravichandran for numerous discussions and many insightful comments during the course of this work. This work was made possible by the financial support of the US Air Force Office of Scientific Research through the Center of Excellence in High Rate Deformation Physics of Heterogeneous Materials (Grant: FA 9550-12-1-0091).

Appendix A

In this appendix, we present solutions to the Riemann problems mentioned in Section 6.1. In order to solve each Riemann problem, the procedure is essentially the same as in Section 4 with minor differences.

A.1. Interface interactions

a. Elastic wave from a purely elastic medium entering a piecewise affine medium

Fig. 14(a) and (b) shows the schematic of such an interaction. As shown in Fig. 14(b), material A is purely elastic while material B is piecewise affine. Depending upon the states a and b in Fig. 14(a), there are three possible cases.

Case 1: *No shock formation*

This happens when either $\sigma_a < \sigma_1$, $\sigma_b \leqslant \sigma_1$ or $\sigma_a > \sigma_1$, $\sigma_b \geqslant \sigma_1$. In this case, the elastic wave passes through the interface without any interruption.

Case 2: *Formation of compression shock*

The compression shock arises when $\sigma_a \leqslant \sigma_1$ and $\sigma_b > \sigma_1$. If $\sigma_a = \sigma_1$, then we have to look at the state just ahead of the point of interaction to decide if case 1 is applicable or case 2. The $X - t$ diagram of this process is presented in Fig. 15(a). The stress state is depicted in Fig. 15(b). The maximal dissipation criteria requires state e to coincide with σ_1. The shock speed U is given by

$$U = \frac{c(-2\sigma_1 + \sigma_a + \sigma_b + c\rho(v_a - v_b))}{-2\sigma_1 + \sigma_a + \sigma_b + c\rho(\varepsilon_c c + v_a - v_b)}.$$

Case 3: *Formation of unloading shock*

This scenario arises when $\sigma_a \geqslant \sigma_1$ and $\sigma_b < \sigma_1$. Like in case 2, if $\sigma_a = \sigma_1$, we have to look at the state ahead of the point of interaction to decide if case 1 is applicable or case 3. The Riemann problem is presented in Fig. 16(a) and (b). In this case, the shock speed is given by

$$U = c - \frac{E\varepsilon_c c}{2\sigma_1 - \sigma_a - \sigma_b + \rho c(\varepsilon_c c - v_a + v_b)}.$$

Notice that state d in Fig. 16(b) can very easily be unloading in nature which can lead to the separation of A–B interface. This allows us to study spallation and re-compression shocks.

b. Compression/unloading shock entering a purely elastic medium

We have already studied the interaction of compression shock at the interface of two piecewise affine materials in Section 4. Now we look at the interaction of compression shock wave at the interface of piecewise affine material and purely elastic material. Fig. 17(a) and (b) depict the interaction. As expected, we get two elastic waves originating from the point of interaction. The state d in material A is given by

$$\sigma_d = \frac{1}{2}(\sigma_1 + \sigma_b + \rho c(v_a - v_b)),$$
$$v_d = \frac{1}{2\rho c}(\sigma_1 - \sigma_b + \rho c(v_a + v_b)).$$

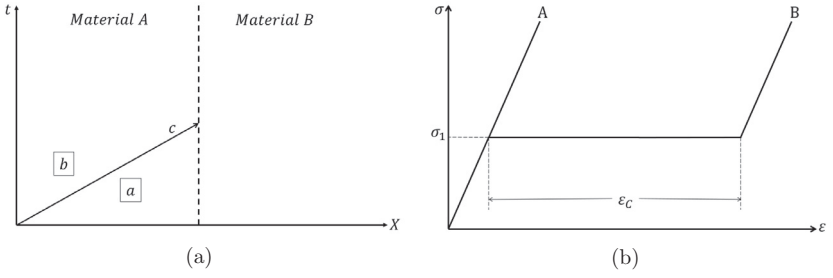

Fig. 14. Schematic diagram of the elastic wave interaction at A–B interface.

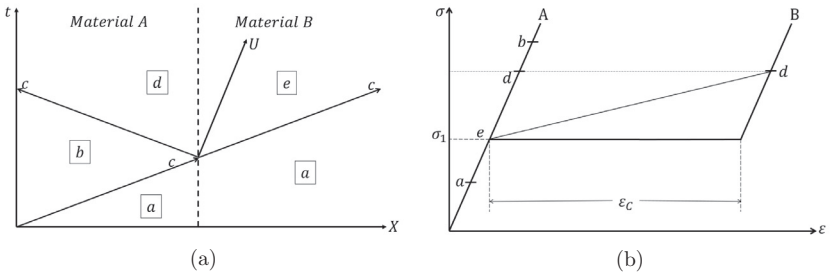

Fig. 15. Elastic wave interaction leading to a compression shock.

The analysis of unloading shock in this case is very similar. The schematic is presented in Fig. 18(a) and (b). The expressions for σ_d and v_d are exactly the same as above.

c. Unloading shock entering another piecewise affine material

The interaction of unloading shock at the interface of two piecewise affine materials results in another unloading shock. The process is exactly the same as described in Section 4. The process is depicted by Fig. 19(a) and (b). The interaction leads to formation of an unloading shock, a receding elastic and forward propagating elastic wave. From our maximum dissipation argument, we know that the forward propagating elastic wave will not exist and state e will coincide with σ_1. The speed of the new unloading shock is given by

$$U_B = c\left(\frac{\sigma_1 - \sigma_b + \rho c(-v_a + v_b)}{\sigma_1 - \sigma_b + \rho c(\varepsilon_c^B c - v_a + v_b)}\right).$$

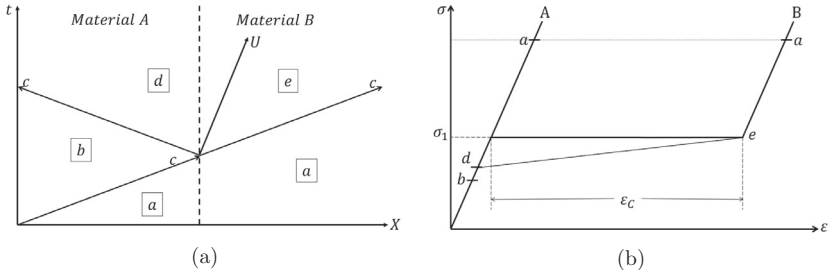

Fig. 16. Elastic wave interaction leading to an unloading shock.

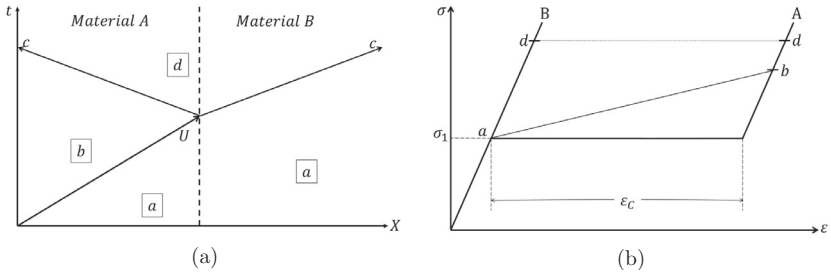

Fig. 17. Compression shock wave entering a purely elastic material.

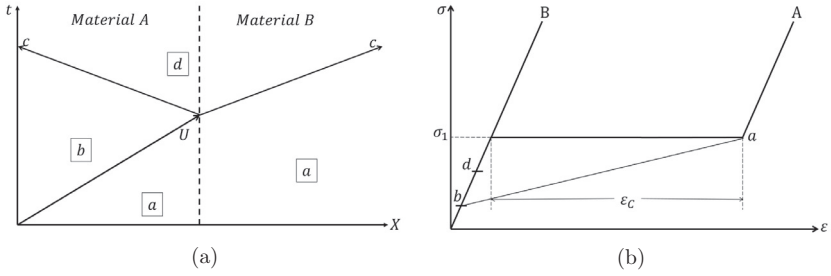

Fig. 18. Unloading shock wave entering a purely elastic material.

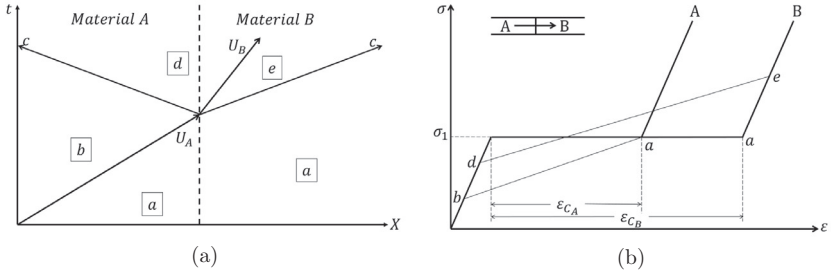

Fig. 19. Unloading shock wave entering another piecewise affine material.

A.2. Wave–wave interactions

a. Interaction of elastic wave and shock wave traveling in the same direction

Next, we study the interaction between an elastic wave and a shock wave in the same direction. Fig. 20(a) and (b) present the schematic of the interaction. The speed of the new shock is given by

$$U_2 = c\left(\frac{-\sigma_1+\sigma_3+\rho c(v_1-v_3)}{-\sigma_1+\sigma_3+\rho c(\varepsilon_c c+v_1-v_3)}\right).$$

The analysis for unloading shock case is exactly the same.

b. Interaction of elastic wave and shock wave traveling in opposite directions

Next, we consider the situation when the waves travel in opposite direction.

Fig. 21(a) depicts the schematic of the Riemann problem under consideration. A shock wave traveling with speed U interacts with an elastic wave traveling in the opposite direction. The Riemann problem involves connecting states 2 and 4 as shown in the figure. Fig. 21(b) and (c) show two possible outcomes of this interaction, which are unloading and compression shocks respectively. Using jump condition and maximal dissipation criteria to solve each case individually, we obtain the following expressions for U_1 and U_2.

$$U_1 = c - \frac{E c\varepsilon_c}{\sigma_2+\sigma_4-2\sigma_1+\rho c(\varepsilon_c c-v_2+v_4)}, \tag{21}$$

$$U_2 = c - \frac{E c\varepsilon_c}{2\sigma_1-\sigma_2-\sigma_4+\rho c(\varepsilon_c c+v_2-v_4)}. \tag{22}$$

Here σ_1 is the yield strength of the material (as in Fig. 3(b)). For the unloading (compression) shock to be applicable, U_2 (U_1) should be from 0 to c. In most of the cases, only one solution is applicable. However, if both shock speeds lie in $(0, c)$, the dissipation values are compared. As explained in Section 7.1, this problem is crucial in the analysis of shock wave propagation.

c. Interaction of two elastic waves in a piecewise affine layer

Now we consider the interaction between two elastic waves in a piecewise affine layer (interaction 2(b) in Section 6.1). Two elastic waves of unloading nature in high strain branch of the stress strain curve can lead to the formation of a pair of unloading shocks. This type of interaction is observed in Fig. 5(a) when the release wave from the impactor interacts with the receding elastic waves in the target. The schematic of the interaction is shown in Fig. 22(a) and (b). The shock speeds U_1 and U_2 are given by

$$U_1 = U_2 = c\,\frac{E\varepsilon_c - \left[E^2\varepsilon_c^2 + (\sigma_3+\sigma_2-2\sigma_1+\rho c(v_3-v_2))^2\right]^{1/2}}{\sigma_3+\sigma_2-2\sigma_1+\rho c(v_3-v_2)}. \tag{23}$$

Similarly, the interaction of two elastic waves (of loading nature) in the low strain branch can lead to the formation of a pair of compression shocks. Fig. 23(a) and (b) show the schematic of such a process. The shock speeds obtained by solving such a Riemann problem are given by

$$U_1 = U_2 = c\,\frac{-E\varepsilon_c + \left[E^2\varepsilon_c^2 + (\sigma_3+\sigma_2-2\sigma_1+\rho c(v_3-v_2))^2\right]^{1/2}}{\sigma_3+\sigma_2-2\sigma_1+\rho c(v_3-v_2)}. \tag{24}$$

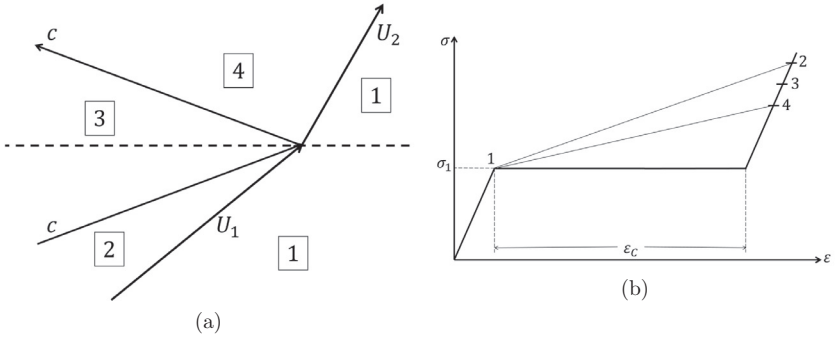

Fig. 20. Interaction of elastic wave with compression shock.

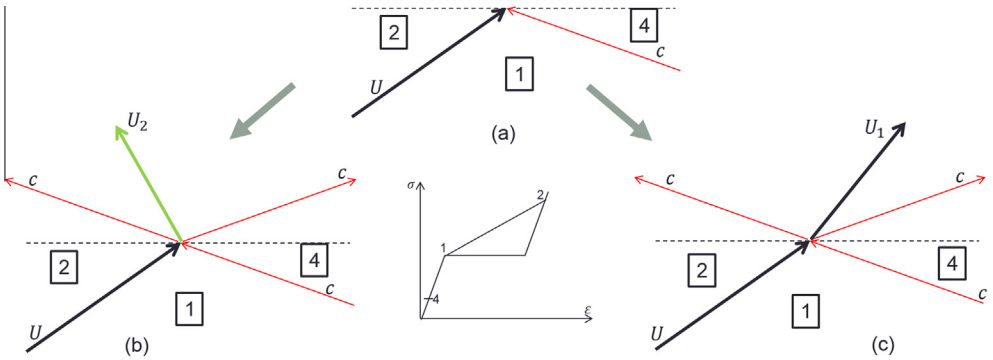

Fig. 21. Interaction between a compression shock and a elastic wave.

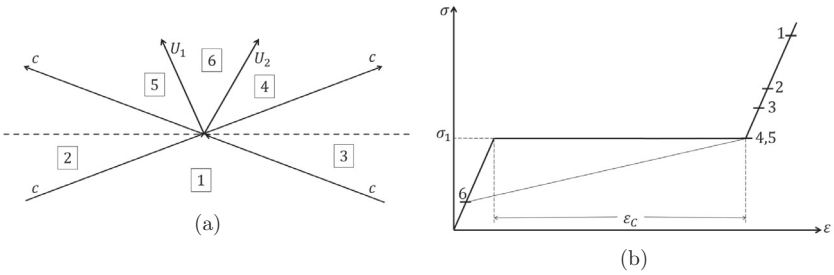

Fig. 22. Interaction of two elastic waves forming a pair of unloading shocks.

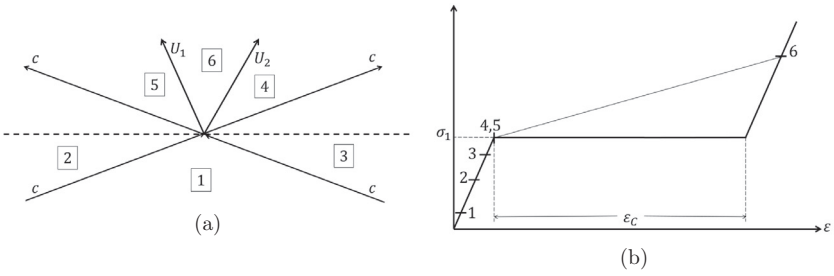

Fig. 23. Interaction of two elastic waves forming a pair of compression shocks.

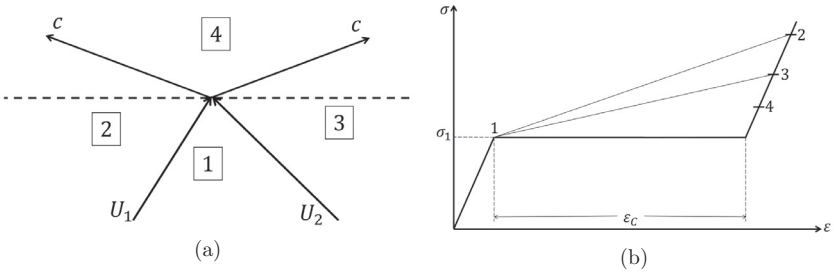

Fig. 24. Interaction of two compression shock waves forming a pair of elastic waves.

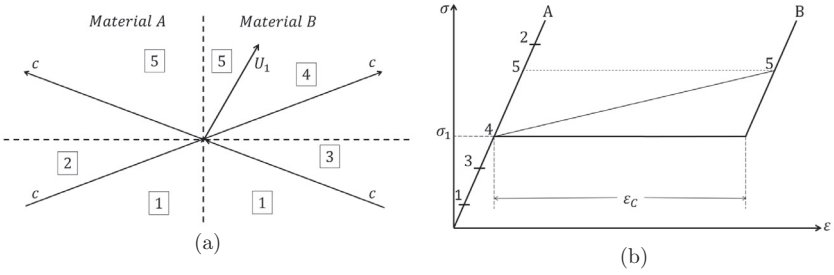

Fig. 25. Interaction of two elastic waves forming a compression shock in the piecewise affine layer.

d. Interaction of two shock waves traveling in opposite direction

Another Riemann problem of concern is the interaction between two shock waves traveling in opposite directions. Fig. 24(a) and (b) show the schematic representation of such a problem involving compression shocks. As expected, the shocks annihilate and form two elastic waves. The jump conditions across the two elastic waves gives us state 4. Similarly, the interaction of two unloading shocks lead to the formation of two elastic waves.

e. Interaction of two elastic waves at the interface of linear and piecewise affine layer

Although a pretty rare event, this becomes important in certain cases like a target with alternate layers of linear and piecewise affine material. This type of interaction can yield shocks in the piecewise affine layer under certain conditions. Fig. 25(a) and (b) show the schematic of the problem where compression shock forms in the piecewise affine layer. Solving the Riemann problem, the shock speed obtained is given by

$$U_1 = c - \frac{Ec\varepsilon_c}{\sigma_2 + \sigma_3 - 2\sigma_1 + \rho c(E\varepsilon_c - \nu_2 + \nu_3)}. \tag{25}$$

Similarly, Fig. 26(a) and (b) represent the case of tensile shock formation. An expression can be obtained for tensile shock speed as follows

$$U_1 = c + \frac{Ec\varepsilon_c}{\sigma_2 + \sigma_3 - 2\sigma_1 - \rho c(E\varepsilon_c + \nu_2 - \nu_3)}. \tag{26}$$

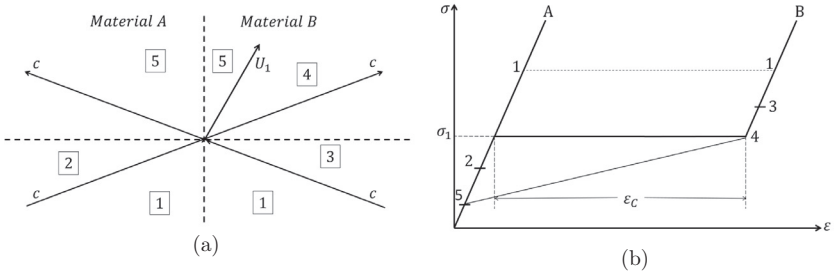

Fig. 26. Interaction of two elastic waves forming a compression shock in the piecewise affine layer.

References

Abeyaratne, R., Knowles, J.K., 1991. Kinetic relations and the propagation of phase boundaries in solids. Arch. Ration. Mech. Anal. 114, 119–154.

Abeyaratne, R., Knowles, J.K., 1992. On the propagation of maximally dissipative phase boundaries in solids. Q. Appl. Math. 50, 149–172.

Armstrong, R.W., Arnold, W., Zerilli, F.J., 2007. Dislocation mechanics of shock induced plasticity. Metallur. Mater. Trans. 38A, 2605–2610.

Asay, J.R., Shahinpoor, M., 1993. High-pressure Shock Compression of Solids. Springer, New York.

Band, W., 1960. Studies in the theory of shock propagation in solids. J. Geophys. Res. 65, 695–719.

Bushman, A.V., Kanel, G.I., Ni, A.L., Fortov, V.E., 1992. Intense Dynamic Loading of Condensed Matter. CRC Press.

Chen, X., Chandra, N., 2004. The effect of heterogeneity on a plane wave propagation through layered composites. Compos. Sci. Technol. 64, 1477–1493.

Chen, X., Chandra, N., Ranjendran, A.M., 2004. Analytical solution to the plate impact problem of layered heterogeneous material systems. Int. J. Solids Struct. 41, 4635–4659.

Clifton, R.J., 1971. On the analysis of elastic/visco-plastic waves of finite uniaxial strain. In: Burke, J.J., Weiss, V. (Eds.), Shock Waves and the Mechanical Properties of Solids. Syracuse University Press, Syracuse, NY, p. 73.

Davison, L., 2008. Fundamentals of Shock Wave Propagation in Solids. Springer, Berlin.

Erzar, B., Forquin, P., 2011. Experiments and mesoscopic modelling of dynamic testing of concrete. Mech. Mater. 43, 505–527.

Grady, D., 1998. Scattering as a mechanism for structured shock waves in metals. J. Mech. Phys. Solids 46, 2017–2032.

Grady, D., 2010. Structured shock waves and the fourth power law. J. Appl. Phys. 107, 013506.

Johnson, J.N., Barker, L.M., 1969. Dislocation dynamics and steady plastic wave profiles in 6061–T6 aluminum. J. Appl. Phys. 40, 4321–4334.

Knowles, J.K., 2002. On the relation between particle velocity and shock wave speed for thermoelastic materials. Shock Waves 12, 137–144.

Knowles, J.K., 2008. On maximally dissipative shock waves in nonlinear elasticity. J. Elasticity 98, 13–23.

Lee, E.H., Yang, W.H., 1973. Waves in composite materials with periodic structure. SIAM J. Appl. Math. 25, 492–499.

Marsh, S.P., 1980. LASL Shock Hugoniot Data. University of California Press, Berkeley.

Meyers, M.A., 1994. Dynamic Behavior of Materials. J. Wiley, New York.

Molinari, A., Ravichandran, G., 2004. Fundamental structure of steady plastic shock waves in metals. J. Appl. Phys. 95, 1718–1732.

Nayfeh, A.H., 1995. Wave Propagation in Layered Anisotropic Media: With Applications to Composites. Elsevier Science, Amsterdam.

Niemczura, J., Ravi-Chandar, K., 2011. On the response of rubbers at high strain rates-II. Shock waves. J. Mech. Phys. Solids 59, 442–456.

Ruoff, A.L., 1967. Linear shock velocity – particle velocity relationship. J. Appl. Phys. 38, 4976–4980.

Ryzhik, L., Papanicolaou, G., Keller, J.B., 1995. Transport equations for elastic and other waves in random media. Wave Motion 24, 327–370.

Rauls, M., Ravichandran, G. Shock wave propagation in heterogeneous materials, in preparation.

Sun, C.T., Achenbach, J.D., Hermann, G., 1968. Continuum theory for a laminated medium. J. Appl. Mech. 35, 467–475.

Swegle, J.W., Grady, D., 1985. Shock viscosity and prediction of shock wave rise times. J. Appl. Phys. 58, 692–701.

Tan, L., Bhattacharya, K. The role of length-scale in propagating boundaries in nonlinear heterogeneous solids, in preparation.

Vogler, T., Clayton, J., 2008. Heterogeneous deformation and spall of an extruded tungsten alloy: plate impact experiments and crystal plasticity modeling. J. Mech. Phys. Solids 56, 297–335.

Vogler, T.J., Borg, J.P., Grady, D., 2012. On the scaling of steady structured waves in heterogeneous materials. J. Appl. Phys. 112, 123507.

Wang, H., Liu, Y., Xia, M., Ke, F., Bai, Y., 2006. Effects of microstructural heterogeneity on the spallation behavior of materials. J. Phys. IV 134, 903–907.

Zhuang, S., Ravichandran, G., Grady, D., 2003. An experimental investigation of shock wave propagation in periodically layered composites. J. Mech. Phys. Solids 51, 245–265.

Zukas, J., 2004. Introduction to Hydrocodes. Elsevier Science.